The 2010 IEEE/RSJ International Conference on
Intelligent Robots and Systems
October 18-22, 2010, Taipei, Taiwan

Development of a Biologically Inspired Multi-Modal Wing Model for Aerial-Aquatic Robotic Vehicles

Richard J. Lock*, Ravi Vaidyanathan, and Stuart C. Burgess

Abstract— **This paper presents a numerical model of a morphing wing supporting the development of a biologically inspired vehicle capable of aerial and aquatic of locomotion. The model draws inspiration from the seabird *Uria aalge*, the common guillemot. It is implemented within a parametric study associated with aerial and aquatic performance, specifically aiming at minimizing energy of locomotion. The implications of varying wing geometry and kinematic parameters are investigated and presented in the form of nested performance charts. Trends within both the aquatic and aerial model are discussed highlighting the implications of parameter variation on the power requirements associated with both mediums. Conflicts of geometric parameter selection are contrasted between the aerial and aquatic model, as well as other trends that impact the design of concept vehicles with this capability. The model has been validated by implementing a heuristic optimization of its key parameters under conditions akin to those of the actual bird; optimal parameters output by the model correlate to the actual behaviour of the guillemot.**

I. Introduction

ADVANCES in fabrication, sensors, electronics, and power storage have made possible the development of a range of small robotic vehicles capable of aerial, terrestrial, and even aquatic locomotion. Additionally, insights into animal locomotion have significantly improved the mobility and stability of these vehicles. At this time, however, the challenges of robotic design for vehicles capable of locomotion through multiple media (e.g. air, water, land) have received considerably less attention in literature. In particular, the design tradeoffs involved between transitioning from aerial to aquatic locomotion modalities for an autonomous robot have yet to be addressed by the research community. Potential applications of such a vehicle include the offshore oil industry, where the vehicle could fly from remote rigs, subsequently diving underwater to inspect pipe work and joints. Another application involves maritime counter-terrorism operations where a boarding crew could launch a small robot to conduct both aerial and aquatic inspection/surveillance of a larger cargo ship. The development of aerial/aquatic multi-modal vehicles would represent a generational leap in robotic utility.

Manuscript submitted March 3, 2010. This work was supported by the UK Engineering and Physical Sciences Research Council (EPSRC) *Richard J. Lock (corresponding author) and Stuart C Burgess are with the Department of Mechanical Engineering at the University of Bristol, Bristol, BS8 1TR, UK ([Richard.Lock;S.C.Burgess]@bristol.ac.uk)
Ravi Vaidyanathan is with the Bristol Robotics Laboratory, Department of Mechanical Engineering at the University of Bristol, Bristol, BS8 1TR, UK and the US Naval Postgraduate School, Monterey, CA, USA, 93943 (r.vaidyanathan@bristol.ac.uk)

Although no mature examples of small robots capable of operation in air and water exist today, many animals have developed multi-use mechanisms that are efficient in both substrates; studying the multi-modal nature of animals can clearly open potential avenues of research. Optimization of competing design tradeoffs between locomotion mechanisms is a particularly ripe area for study.

This work documents the initial stages of research to further our understanding of avian mechanisms enabling both aerial and aquatic locomotion. A detailed numerical model of a wing transitioning from aerial to aquatic locomotion is developed to reproduce the compromises balanced by these animals, such that the outcomes can be utilised in future vehicle concept designs. A genetic algorithm (GA) is then implemented to balance competing tradeoffs based on desired performance characteristics. Results are validated through comparison to the natural (bird) system. The evolutionary optimization tool is then implemented to produce designs for varying performance criteria for robots performing aerial/aquatic missions.

II. Avian Inspired Aerial/Aquatic Performance

Imagine a vehicle that could not only fly great distances, but also swim under water with the same propulsion system by morphing the shape of the wing. This is, in essence, what the auk family of seabirds accomplishes. The common guillemot, *Uria aalge*, nests in coastal areas but hunts several kilometres out to sea [1]. Once at the hunting ground the birds dive underwater, morphing their wings and utilise the same flapping mechanism in water as they do in air but with a reduced flapping frequency (9 Hz to 2.5 Hz) and reduced forward velocity (19.1 m/s to 1.5 m/s) [2],[3]. The alteration in wing shape can be seen in Fig. 1. This ability is currently unmatched within the engineering world and as such offers a challenging task in trying to understand and reproduce this technique.

Fig. 1. Guillemot during aerial and aquatic locomotion (adapted from unpublished BBC footage)

We have developed a model of this behaviour through a combination of hydrodynamic and inertial dynamic formulations, an indication of likely thrust generation, a derivation of the required driving torques associated with the aquatic flapping motion, and derivation of subsequent power requirements for aquatic locomotion. Known formulae relating to avian flight are simultaneously utilised in order to determine the power requirements of aerial locomotion based on geometric variations. The implications of variations in both geometric and kinematic parameters on power requirements are investigated with the subsequent trends and conclusions presented in a parametric study.

III. MODELLING OF A MULTI-MODAL WING DESIGN

A. Aquatic Operations

A simplified representation of the foil orientation during aquatic locomotion is proposed. Fig. 2 displays the axes and subsequent sign conventions that accompany the foil model, in keeping with the standard format used in AUV design [4].

In addition to the body-fixed axes (XYZ), an additional set of axes are attached to the flapping wing (xyz), coincident with the body-fixed axes when the roll, pitch and retraction angle of the foil are zero. These axes are considered to rotate with the wing during roll motion. The hydrodynamic model used during simulation is based on quasi-steady blade element theory. For each geometric arrangement the wing is split into finite segments in the span-wise direction which are analyzed independently based on the local conditions [5].

In order to utilise blade element theory (BET), fully described kinematics must be known for the wing throughout the wing beat cycle. The kinematic trajectory of the foil was chosen to be similar to that of the common guillemot, utilising a two degree of freedom flapping motion consisting of roll and pitch operating in a harmonic motion with the same circular frequency ω (rad/s) [6]. The roll motion is governed by:

$$\phi(t) = \phi_0 \sin(\omega t), \quad (1)$$

where ϕ_0 is the maximum roll amplitude in radians. Similarly the pitch motion is governed by:

$$\theta(t) = \theta_0 \sin(\omega t + \psi), \quad (2)$$

where θ_0 is the maximum pitch amplitude in radians and ψ is the phase angle between pitch and roll. It has been highlighted in previous research that a phase lag of 90° is the most suitable arrangement which shall be adhered to here [7]. This results in equation (2) changing to:

$$\theta(t) = \theta_0 \cos(\omega t) \quad (3)$$

Knowing maximum roll amplitude and pitching amplitude the kinematics of the flapping foil are fully described. This is graphically shown in Fig. 3.

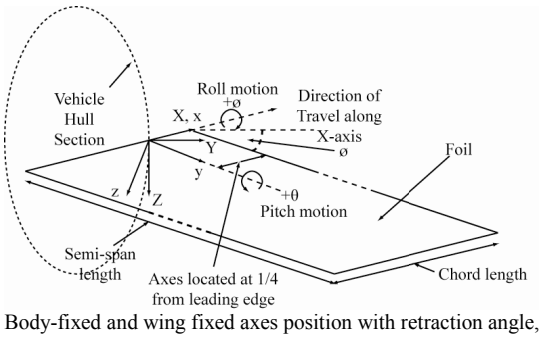

Fig. 2. Body-fixed and wing fixed axes position with retraction angle, β = 0

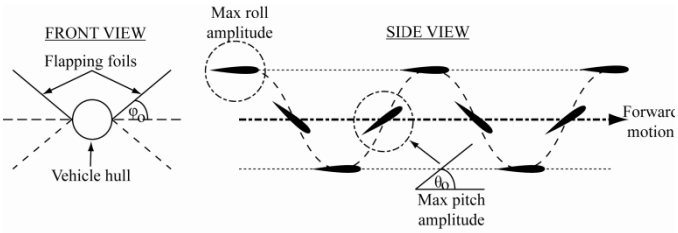

Fig. 3. Graphical representation of harmonic nature of the roll and pitch motions, demonstrating phase lag of maximum roll and pitch amplitudes

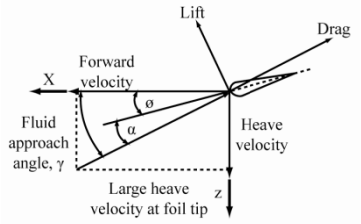

Fig. 4. Fluid approach angle and effective angle of attack relative to heaving and pitching motions and forward velocity of foil

Previous research into flapping foils models each blade element with a heave like motion [8]. Subsequently if the forward velocity of the foil is known and the heave velocity is calculated for each element, the fluid approach angle, γ, can be calculated based on these values, as shown in Fig. 4. The instantaneous pitch angle at each element is also required to determine the effective angle of attack that each blade element experiences. This can again be seen in Fig. 4.

For every blade element, each with its own kinematic characteristic, the lift and drag are determined by the following:

$$dL = 0.5\rho V_{res}^{\ 2} dSC_l, \quad (4)$$

$$dD = 0.5\rho V_{res}^{\ 2} dSC_d \quad (5)$$

where dL is the lift associated with a specific element, dD is the drag associated with that element, ρ is the density of the water, V_{res} is the resultant velocity due to both the forward velocity and heave velocity, dS is the characteristic area and C_l and C_d are the lift and drag coefficients respectively based on the specific foil arrangement.

The lift coefficient and drag coefficient varies according to the effective angle of attack that each element is experiencing; therefore a relationship between the angle of attack and the lift and drag coefficients must be determined. To do this the lift and drag coefficient profiles are mapped to a harmonic profile [9]. Equations 4 and 5 subsequently become:

$$dL = 0.5\rho V_{res}^{\ 2} dSC_{L\max} \sin(2\alpha) \quad (6)$$

$$dD = 0.5\rho V_{res}^{\ 2} dSC_{D\max} (1 - \cos(2\alpha)) \quad (7)$$

The lift and drag forces are then calculated for the whole foil. A rotational transformation is needed in order to

develop an overall picture of the forces experienced through the entire flapping motion. As the foil model moves along the X-axis, lift and drag components of each element along the X-axis can be determined by simple trigonometry. Similar transformations are done for the Y- and Z-direction. However, in addition to resolving the forces in relation to the fluid approach angle, they must again be resolved based on the position due to the roll motion.

Each blade's hydrodynamic moment can also be calculated about the body fixed axes based on the localised forces experienced at each element and the distance from the point of rotation. Summating these over the semi-span length provides the overall hydrodynamic moments. In addition to the forces and moments acting about the body fixed axes, the forces must also be resolved about the wing fixed axes, xyz. This is again performed by a rotational transformation.

Inertial dynamics must also be considered for the foil. In order to develop a generic inertia tensor that could be utilised for the various geometric arrangements the wing was assumed to be the equivalent of a specific thickness flat plate. The generic inertia tensor was determined for the flat plate based on the geometric variables shown in Fig. 5, which shall subsequently be referred to as I_{RB}.

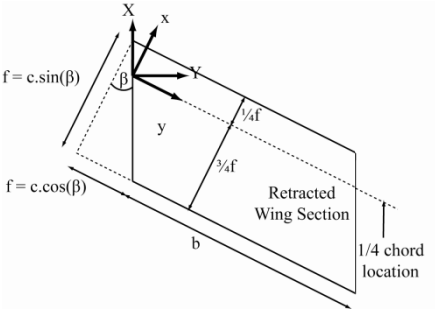

Fig. 5. Flat plate representation of foil with assumed constant thickness

Consideration must also be given to the inertia associated with the surrounding fluid set in motion due to the flapping foil. Inviscid flow theory shows that the added mass of a foil accelerated in a perpendicular direction to its chord is equal to an imaginary circular cylinder encapsulating the wing, with the chord as its diameter [10]. It can be assumed that the foil has an added mass per unit span equal to:

$$m_a = \frac{1}{4}\rho_{water}\pi c^2 \tag{8}$$

where ρ_{water} is the density of water and c is the chord width of the foil being analysed. To calculate the overall inertia tensor associated with the added mass the foil was again considered as finite strips. Each strip was then assigned an equivalent cylindrical mass as described by equation 8. This was then treated as a point mass located at the centre of the foil, placed at the equivalent half chord location of each segment. As the moments and products of inertia of each point mass are calculated with respect to the wing fixed axes, these can be combined for the entire added mass associated with the wing. This overall value represents I_A for any foil geometry arrangement, and as I_{RB} and I_A are calculated about the same axes the values can be summated to provide the overall inertia tensor to be used when calculating the inertial dynamics of the system.

The angular velocities and accelerations of the wing can be calculated by considering the Euler angles due to the three rotations; pitch, roll and retraction angle. Firstly, a rotation is experienced about the X axis corresponding to the roll of the wing, secondly, a rotation due to the pitching moment and finally, the rotation due to the retraction angle β, providing an overall transformation of:

$$[R] = [R_\beta][R_\theta][R_\phi] \tag{9}$$

The overall angular velocity can be calculated based on the vector sum of the individual rotation rates, leading to angular velocities and angular acceleration about the wing fixed xyz axes as:

$$\begin{aligned}\underline{\omega} &= \left(\dot{\phi}\cos\beta\cos\theta - \dot{\theta}\sin\beta\right)\underline{i} \\ &+ \left(\dot{\theta}\cos\beta - \dot{\phi}\sin\beta\cos\theta\right)\underline{j} \\ &+ \left(\dot{\phi}\sin\theta\right)\underline{k}\end{aligned} \tag{10}$$

$$\begin{aligned}\underline{\alpha} &= \left(\ddot{\phi}\cos\beta\cos\theta - \ddot{\theta}\sin\beta - \dot{\theta}\dot{\phi}\sin\theta\cos\beta\right)\underline{i} \\ &+ \left(\ddot{\theta}\cos\beta - \dot{\theta}\dot{\phi}\sin\theta\sin\beta - \ddot{\phi}\sin\beta\cos\theta\right)\underline{j} \\ &+ \left(\ddot{\phi}\sin\theta + \dot{\theta}\dot{\phi}\cos\theta\left(\cos^2\beta - \sin^2\beta\right)\right)\underline{k}\end{aligned} \tag{11}$$

Utilising the inverse of the rotation matrix governed by equation 9 the angular velocities and angular accelerations about the body fixed XYZ axes can be calculated:

$$\underline{\omega}_{XYZ} = [R]^T\,\underline{\omega}_{xyz} \tag{12}$$

$$\underline{\alpha}_{XYZ} = [R]^T\,\underline{\alpha}_{xyz} \tag{13}$$

The torque experienced about the xyz axes can be calculated based on the rate of change of angular momentum, and as the wing is assumed rigid, the inertia tensor remains constant so that the torque experienced about the wing fixed xyz axes is:

$$\underline{\tau}_{xyz} = \dot{\underline{H}}_{xyz} = I_{xyz}\,\underline{\alpha}_{xyz} \tag{14}$$

A similar process is used to determine the torques experienced about the body fixed XYZ axes with one key difference. The inertia tensor is calculated based on the wing fixed axes location so that the inertia tensor associated with the body-fixed XYZ axes changes over time.

As the inertia tensor is a tensor of the second rank, a similarity transformation must be used when dealing with rotations. Also, as the rotation matrix relates the XYZ axes to the xyz axes, the inverse of the transformation must be used to transform the inertia tensor about the xyz axes to that about the XYZ axes. This is done by the following:

$$I_{XYZ} = [R]^T[I_{xyz}][R] \tag{15}$$

By combining equations 13 and 15 the torques about the body fixed XYZ axes can be calculated by:

$$\tau_{XYZ} = \dot{\underline{H}}_{XYZ} = [R]^T[I_{xyz}][R]\cdot[R]^T\,\underline{\alpha}_{xyz} \tag{16}$$

Having calculated the hydrodynamic forces and the inertial contributions relating to the motion of the wing,

simplified equations of motion can represent the system.

For the purposes of numerical simulation, the linear forward velocity of the foil is assumed to be constant. The assumption is therefore made that the wing is only undergoing angular accelerations due to the pitch and flapping motions. Therefore there is no linear acceleration experienced by the wing and all inertial components come from rotational rather than translational motions. Coriolis and centripetal term and the damping matrix were judged to be negligible for the system model. Finally, the wing is assumed neutrally buoyant which subsequently allows the gravitational terms to be disregarded. The simplified equation of motion about the wing fixed axes xyz can therefore be represented by:

$$I_{xyz}\underline{\alpha}_{xyz} = \tau_{motor\_y} + \tau_{hydro-xyz} \quad (17)$$

where τ_{motor_y} is the motor torque required for the pitching motion and $\tau_{hydro\text{-}xyz}$ is the hydrodynamic torque contribution, with the same being true for the roll motion about the body fixed XYZ axes:

$$I_{XYZ}\underline{\alpha}_{XYZ} = \tau_{motor\_X} + \tau_{hydro-XYZ} \quad (18)$$

where τ_{motor_X} is the torque required for flapping motion and $\tau_{hydro\text{-}XYZ}$ is the hydrodynamic torque about XYZ axes.

Knowing the torques experienced due to the roll motion and pitch motion of the foil, and the angular velocities of both motions, an indication of the power to drive each motion can be formed:

$$P(t) = \tau(t)\cdot\omega(t) \quad (19)$$

Subsequently a time averaged power requirement $\overline{P_X}$ and $\overline{P}_y$ can be deduced for specific geometric arrangements for both the flap and pitch motion. Combining these provides an indication of the total power required by the system:

$$\overline{P}_f = \overline{P}_X + \overline{P}_y \quad (20)$$

This can therefore be calculated for any combination of geometric and kinematic parameters.

B. Aerial operations

During flight, the vehicle must overcome external forces in order to maintain steady horizontal flight. By determining these, the overall power requirement for flight can be calculated. These forces can be broken down into three distinct forms of drag that the vehicle is subjected to [11].

The first component is induced drag. The value of induced drag can be calculated by using the following:

$$Induced\ drag = \frac{2k_{induced}m^2g^2}{\pi\rho_{air}U^2b^2} \quad (21)$$

where $k_{induced}$ is the induced drag factor, m is the mass of the vehicle (kg), g is the gravitational constant, U is the air velocity (m/s), ρ_{air} is the density of air (kg/m^3) and b is the wingspan (m).

The second component is that associated with the profile drag of the aerofoil, made up of skin friction and pressure drag. Profile drag is approximated by the following, where S is the wing area (m^2) and $C_{D\text{-}Pro}$ is the profile drag coefficient:

$$\mathrm{Pr}ofile\ drag = 1/2\,\rho_{air}SU^2C_{D-\mathrm{Pr}o} \quad (22)$$

The final form of drag experienced is that of parasitic drag. This refers to the drag associated with the non-thrust producing parts of an airborne system, i.e. the fuselage in an aircraft [13]. This can be calculated using the following, where S_b is the frontal area of the body (m^2) and $C_{D\text{-}Bod}$ is the body drag coefficient:

$$Parasitic\ drag = 1/2\,\rho_{air}S_bU^2C_{D-Bod} \quad (22)$$

Utilising the fact that power is the product of force and velocity, multiplying each by the mean airspeed allows the power associated with each drag force to be calculated.

$$P_{Ind} = 2km^2g^2/\pi\rho_{air}U\,b^2 \quad (23)$$

$$P_{\mathrm{Pr}o} = 1/2\,\rho_{air}SU^3C_{D-\mathrm{Pr}o} \quad (24)$$

$$P_{Par} = 1/2\,\rho_{air}S_bU^3C_{D-Par} \quad (25)$$

$$P_{Sum} = P_{Ind} + P_{\mathrm{Pr}o} + P_{Par} \quad (26)$$

For any given wing arrangement, the air velocity that gives the minimum power per unit time, can be found by differentiating P_{sum} with respect to velocity. Once this value is known, the equivalent total power at this velocity can subsequently be determined with various geometric wing arrangements. The implications of varying geometric parameters are discussed in the following section.

IV. MULTI-MODAL PARAMETRIC STUDY OF WING DESIGN

A. Multi-Modal Wing Parameters

The implications of variations in both geometric and kinematic parameters associated with the foil are investigated with the aim of elucidating trends that can aid in subsequent vehicle designs. These parameters can be found within table 1. The aim is to minimize the cost of the mission by minimizing power requirements. Drawing from equations 20 and 26 allows this to be quantified for both aquatic and aerial operations.

B. Aquatic Parametric Study

The implications on power requirements of varying kinematic parameters for an individual geometric arrangement are presented in Fig. 6.

It was found that the optimum pitch angle for a specific geometric arrangement varies depending on the kinematic parameters. From a future design perspective, this highlights the need for adjustable pitch for flapping foils operating with under constrained kinematics.

Although not graphically shown here, it was found that at a fixed flapping frequency greater thrust is generated by the flapping foils at lower speeds highlighting the need to carefully select kinematic parameters, tuned for specific operating conditions. Further more, increasing the flapping frequency was seen to decrease the sensitivity of the maximum pitch amplitude required to generate high thrust. In each case increasing the maximum roll amplitude $\varphi_{0,}$ up to the maximum constrained value of 45°, results in an increase in the thrust generated. The associated power

requirements, which have been constrained based on solutions that produce positive thrust, can be seen to increase with increases in φ_0, f and U_f.

Initial simulations investigating the trends in geometric variations identified that the semi-span length had greater implications on thrust generation and power requirements during flapping motion than chord length; the foil was therefore fixed at an aspect ratio of 8, to allow further trends to be elucidated between wing-span, b and retraction angle, β. The resulting power requirements are presented in Fig. 7, where the forward velocity, U_f and flapping frequency f have been set at 1.0 m/s and 1.5 Hz respectively.

Further trends have been elucidated from the implications of varying the semi-span length and retraction angle. The sensitivity of the thrust production to maximum pitch amplitude decreases as the semi-span increases. This trend also remains when the foil is subjected to retraction angles up to the maximum 45°.

As the retraction angle increases, the foils thrust generating ability decreases, but also results in a reduction in the power, however it was found that the reduction in thrust generation is less than the reduction in power. This trend increases with semi-span. At a semi-span of 0.3, a retraction angle of 45° results in a 72% decrease in thrust, with a 76% reduction in power requirement. At a semi-span of 0.5, a retraction angle of 45° results in a 70% decrease in thrust compared to a 76% reduction in power requirement. This highlights the benefit of introducing a large retraction angle in future concept designs.

C. *Aerial Parametric Study*

The implications of variations in vehicle geometry are all investigated in order to establish overall trends within the aerial model. The overall findings are presented in Fig. 8.

Conversely to the aquatic model, the power requirement, P_{sum} decreases as the span length is increased. As the square of the span length is in the denominator of the formula, the larger the span the lower this term will be, hence resulting in a benefit from a large wing span.

The opposite is true for the chord length, which when increased results in an increase in power requirement. This indicates a long narrow wing would be most beneficial in reducing the cost of transport.

The vehicle hull size, $\varnothing_h$, which results in the frontal area, S_b, effects the overall power requirements but only slightly, identifying the lack of dominance of equation (25) on the overall power requirements. However, of much greater importance is the overall mass of the vehicle. Increasing the mass from 0.5 kg to 1.5kg results in a large increase in power required, again explained by the dominance of equation (23) on the overall power requirements, where the mass term appears in the numerator, raised to the power of two. Conversely to the span, an increase in mass results in a quadratic increase in power requirements provided all other parameters remain the same.

TABLE 1
PARAMETERS AND OUTPUTS

Variables		Outputs
Geometric	Kinematic	
Span length, b	Max roll amplitude, φ_0	Aquatic thrust, T
Chord length, c	Max pitch amplitude, θ_0	Aquatic flapping foil power requirements, P_f
Retraction angle, β	Flapping frequency, f	Overall aerial power requirements, P_{sum}
Vehicle mass, m	Aquatic forward velocity, U_f	
Hull diameter, $\varnothing_h$		
Vehicle frontal area, S_b		

V. INITIAL MODEL VALIDATION AND APPLICATION

Due to the novelty of the requirement for operations in air and water it is difficult to validate the numerical model with current vehicle designs. However, the biological examples from which inspiration is taken can be used for initial validation purposes. To do this the typical behaviour of the

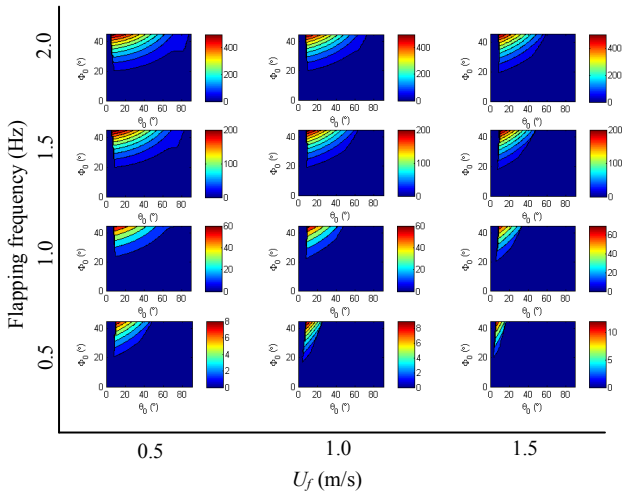

Fig 6: Nested performance chart with contours representing power required (W), by a foil with a fixed 0.4m semi-span and 0.1m chord length. Continuous nested axes represent max roll, φ_0 and pitch amplitudes, θ_0. Discretized axes represent aquatic forward velocity, U_f and flapping frequency, f

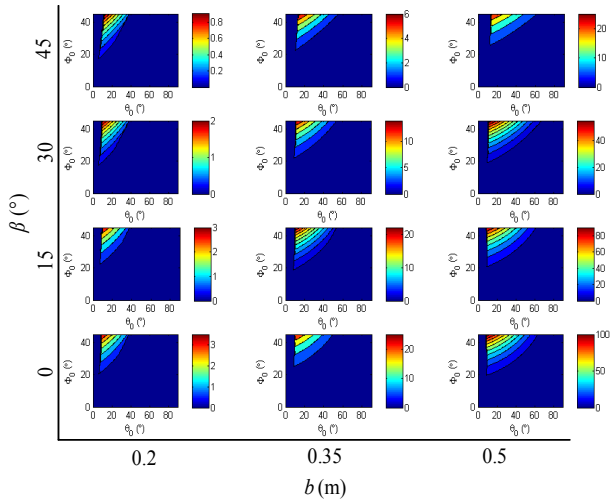

Fig 7: Nested performance chart with contours representing power required (W), by a foil at a fixed U_f = 1.0 m/s and f = 1.5Hz. Continuous nested axes represent max roll, φ_0 and pitch amplitudes, θ_0. Discretized axes represent semi-span length, b/2, and retraction angle, β.

TABLE 2
VARIOUS MISSION CRITERIONS ALONG WITH OPTIMAL WING GEOMETRY

Mission	Aerial Range (km)	Aerial Velocity (m/s)	Aquatic Range (km)	Aquatic Velocity (m/s)	Wing span (m)
Common Guillemot [1] [3]	2	20	0.5	1.5	0.71
Simulated Guillemot	2	20	0.5	1.5	0.79
Counter-Terrorism	1	12.5	500	1	0.83
Oil platform Deployment	0.5	20	1	1.5	0.78
Search and Rescue	1	25	500	1	0.53

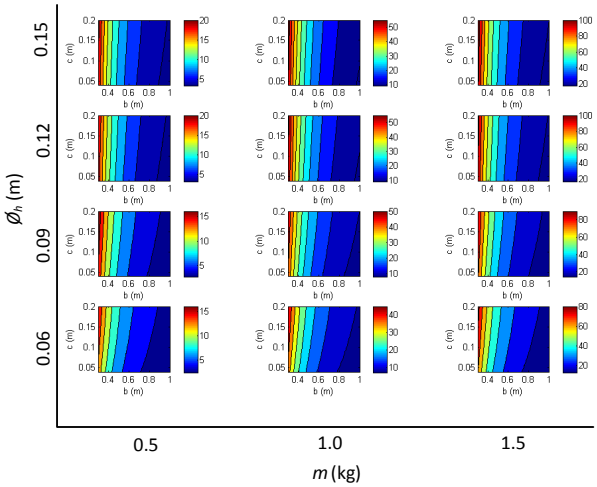

Fig. 8. Nested performance chart with contours representing minimum power (W) required by a wing based on specific minimum power velocities. Continuous nested axes represent span, *b* and chord, *c*. Discretized axes represent mass, *m* and vehicle hull diameter, $Ø_h$.

common guillemot is utilised in a mission based investigation.

Knowing the typical ranges of common guillemots in both substrates, the aerial and aquatic models can be combined to determine the total energy cost of the mission. A mission based on [1] and [12] is detailed in table 2.

The same mission was then used in the optimization process, under suitable geometric and kinematic constraints. It can be seen that the GA suggests an optimal wing span approximately equal (≈ 10% larger) to that of the guillemot for equivalent missions providing initial validation of the numerical model. The cost function of the GA is based on the specific power requirements of the aerial and aquatic phases, with the overall energy cost then calculated by multiplying the power requirements by the time length in which each mission phase would be completed.

Several hypothetical missions, such as marine counter-terrorism operations, oil platform deployment and littoral search and rescue missions have also been considered. A summary of the results for these various missions are presented in table 2 along with the comparison with the common guillemot. The optimal wing span to use can be seen to vary based on the specific mission criterion relating to aerial and aquatic ranges and velocities. Future work aims to elucidate trends from the kinematic conditions suggested by the model for varying mission criterion.

VI. CONCLUSIONS

The initial conclusions that can be elucidated from the study for aerial/aquatic locomotion are:

- Under-constrained vehicle kinematics are vital in roll and pitch motion.
- Major conflicts exist in wing span selection due to converse implications on power requirements of both aerial and aquatic modes of locomotion.
- Retraction angle β has a beneficial effect on overall performance considering the thrust generation *versus* power requirements.
- Minimising overall vehicle mass of great importance in reducing aerial power requirements.
- Simulated guillemot mission provides initial validation of presented numerical model.

Future work will investigate further mission specific implications on parameter selections and validate the current findings through experimental work. The presented model shall be used as an initial design tool in this process, leading towards a specific mission based vehicle design.

ACKNOWLEDGMENT

The authors acknowledge the support of the UK Engineering and Physical Sciences Research Council (EPSRC) Doctoral Training Assistantship (DTA) Program.

REFERENCES

[1] A. J. Gaston, The Auks: Bird Families of the World (Series 5). Oxford: Oxford University Press, 1998.
[2] J. R. Lovvorn, D. A. Croll and G. A. Liggins, “Mechanical *versus* Physiological Determinants of swimming speeds in diving Brunnicj’s Guillemots”. *Journal of Experimental Biology*. 202, 1741-1752 (1999)
[3] C. J. Pennycuick, “Flight of Auks (Alcidae) and other northern seabirds compared with southern procellariiformes: Ornithodolite observations”. *Journal of Experimental Biology*. 128, 335-347 (1987)
[4] T. I Fossen, Guidance and Control of Ocean Vehicles. Chichester, West Sussex: John Wiley & Sons Ltd, 1999.
[5] C. A. Hui, “Penguin swimming. I. Hydrodynamics”. Physiol. Zool 61(4): 333-343, 1988
[6] L. C. Johansson, L. C. and B. S. W. Aldrin, "Kinematics of diving Atlantic puffins (Fratercula arctica L.): evidence for an active upstroke.”*Journal of Experimental Biology* 205: 371-378, (2002)
[7] D. A. Read, F. S. Hover, and M. S. Triantafyllou. "Forces on oscillating foils for propulsion and maneuvering." *Journal of Fluids and Structures* 17: 163-183. (2003).
[8] A. H. Techet, "Propulsive performance of biologically inspired flapping foils at high Reynolds numbers." *Journal of Experimental Biology* 211: 274-279. (2008)
[9] C. Georgiades, M. Nahon and M. Buehler. "Simulation of an underwater hexapod robot." *Ocean Engineering* 36: 39-47. (2009)
[10] C. P. Ellington. "The aerodynamics of hovering insect flight. II. Morphological parameters." *Phil. Trans. R. Soc*. Lond. B 305: 17-40. (1984)
[11] U. M Norberg, "Vertebrate Flight: Mechanics, Physiology, Morphology, Ecology and Evolution." Zoophysiology Vol 27. Springer-Verlag, Berlin, Germany. (1990).
[12] J. R. Lovvorn, G. A. Liggins, M. H. Borstad, S. M. Calisal and J. Mikkelsen. "Hydrodynamic drag of diving birds: effects of body size, body shape and feathers at steady speeds." *Journal of Experimental Biology* 204: 1547-1557. (2001)
[13] S. Vogel; “Life in moving fluids”. Princeton, N.J.: Princeton University Press (1994)
[14] S. Burgess, D. Pasini and K. Alemzadeh. “Improved visualisation of the design space using nested performance charts.” *Design Studies* 25: 51-62. (2004)